The Astrophysical Journal, 714:1133–1141, 2010 May 10 doi:10.1088/0004-637X/714/2/1133

MULTI-SPACECRAFT OBSERVATIONS OF THE 2008 JANUARY 2 CME IN THE INNER HELIOSPHERE

X. H. Zhao[1], X. S. Feng[1], C. Q. Xiang[1], Y. Liu[2], Z. Li[1,3], Y. Zhang[4], and S. T. Wu[5]
[1] SIGMA Weather Group, Sate Key Laboratory of Space Weather, Center for Space Science and Applied Research, Chinese Academy of Sciences, Beijing 100190, China; xhzhao@spaceweather.ac.cn
[2] Space Sciences Laboratory, University of California, Berkeley, CA 94720, USA
[3] Graduate University of the Chinese Academy of Sciences, Beijing, China
[4] Institute of Geology and Geophysics, Chinese Academy of Sciences, Beijing 100029, China
[5] Center for Space Plasma and Aeronomic Research and Department of Mechanical Engineering, University of Alabama in Huntsville, Huntsville, AL 35899, USA
Received 2010 January 9; accepted 2010 March 17; published 2010 April 16

ABSTRACT

We perform a detailed analysis of a coronal mass ejection (CME) on 2008 January 2. The combination of the *Solar and Heliospheric Observatory* and the twin *STEREO* spacecraft provides three-point observations of this CME. We track the CME in imaging observations and compare its morphology and kinematics viewed from different vantage points. The shape, angular width, distance, velocity, and acceleration of the CME front are different in the observations of these spacecraft. We also compare the efficiency of several methods, which convert the elongation angles of the CME front in images to radial distances. The results of our kinematic analysis demonstrate that this CME experiences a rapid acceleration at the early stage, which corresponds to the flash phase of the associated solar flare in time. Then, at a height of about 3.7 solar radius, the CME reaches a velocity of 790 km s^{-1} and propagates outward without an obvious deceleration. Because of its propagation direction away from the observers, the CME is not detected in situ by either *ACE* or *STEREO*.

Key words: solar–terrestrial relations – solar wind – Sun: coronal mass ejections (CMEs)

Online-only material: color figures

1. INTRODUCTION

Coronal mass ejections (CMEs), referring to large-scale eruptions of plasma and magnetic field which propagate from the Sun into interplanetary space, are one of the most ferocious events in the solar atmosphere. When colliding with the Earth's magnetosphere, CMEs can produce severe geomagnetic storms if they have a sustained southward magnetic field component. Since their discovery in the 1970s, CMEs have been the focus of extensive studies from both solar and space scientists. However, up to now our knowledge about their physical characteristics has remained limited. CMEs are usually observed by white-light coronagraphs, which provide the integrated intensity along the line of sight. The coronagraph observations give only the projected view of CMEs on the plane of sky (POS), perpendicular to the Sun–observer line. The observed parameters, such as the morphology, angular width, propagation distance, velocity, and acceleration, inevitably suffer from the projection effects. Therefore, single point observations cannot provide the three-dimensional (3D) structure and kinematics of CMEs (Howard et al. 1985; Hundhausen 1993; St. Cyr et al. 2000; Temmer et al. 2009). Many methods and techniques have been developed to correct for projection effects and infer the 3D morphology and kinematics of CMEs (Sheeley et al. 1999; Zhao et al. 2002; Michalek et al. 2003; Xie et al. 2004; Michalek 2006; Howard et al. 2008; Frazin et al. 2009). Because previously there has only been a single vantage point for observations, these methods are usually based on some assumptions or approximations. In addition, during the *Solar and Heliospheric Observatory* (*SOHO*) era, CMEs could only be tracked up to 32 Rs (solar radius), which is the upper limit of the field of view (FOV) of the Large Angle Spectrometric Coronagraph (LASCO).

The launch of the *Solar TErrestrial RElations Observatory* (*STEREO*) in 2006 heralded a new epoch for the observations of CMEs. *STEREO* consists of twin space-based observatories with identical instruments. The two spacecraft are positioned in two orbits around the Sun, with one ahead (A) and the other behind (B) the Earth. They are drifting away from the Earth at a rate of approximately 22.°5 per year. Superior to *SOHO*, *STEREO* can observe the Sun–Earth space from two different points off the Sun–Earth line. The Sun Earth Connection Coronal and Heliospheric Investigation (SECCHI) aboard *STEREO* is composed of five imaging telescopes including EUVI, COR1, COR2, HI1, and HI2, which together can track a CME from the solar corona to 1 AU (Howard et al. 2008). Studies based on the observations of *STEREO* have been carried out to remove, at least partially, the projection effects and acquire the kinematics of CMEs in a 3D space (e.g., Harrison et al. 2008; Howard & Tappin 2008; Mierla et al. 2008; Liu et al. 2010; Temmer et al. 2009; Thernisien et al. 2009; Maloney et al. 2009; Wood et al. 2009a, 2009b; Webb et al. 2009). In this paper, we compare in detail the observed characteristics of a CME by multiple spacecraft including *STEREO-A*, *STEREO-B*, and *SOHO*. This CME has a particular source location and propagation direction so that *STEREO*'s observations give a relatively good estimate of its real 3D characteristics. We apply three methods to convert the elongation angles of the CME front in imaging observations to radial distances, and select the one that we think best denotes the true distance. Based on the results, the kinematic development of this CME within 60 solar radii of the Sun is analyzed. Our study demonstrates how multiple spacecraft observations can provide a much better characterization of the morphology and kinematics of CMEs than the previous L1 observations alone can.

2. IMAGING THE EVENT

By 2008 January 2, the date of the CME of interest, the longitudinal separation between *STEREO-A* and *B* had reached 44° as shown in Figure 1. Data from other spacecraft used

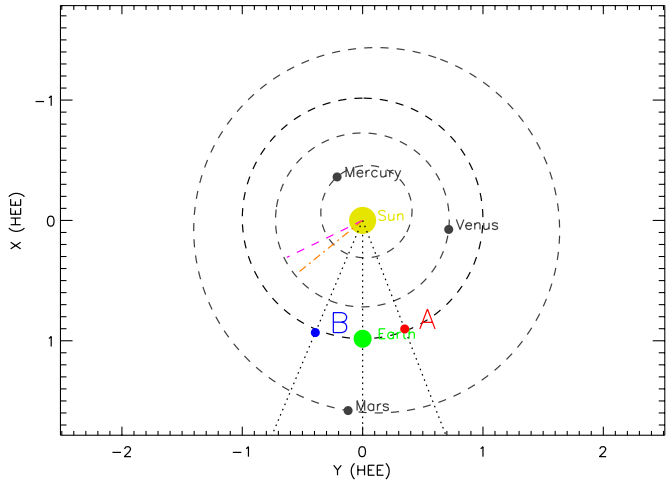

Figure 1. Locations of the Sun, Earth, *STEREO-A*, and *STEREO-B* on 2008 January 2 in heliocentric Earth ecliptic coordinates. The orbits of Mercury, Venus, and Mars are also shown. The red-dashed line and dash-dotted line through the Sun center denote the directions of this CME (E64 and E51), which are estimated, respectively, by the mass model and forward model of the CME (Thernisien et al. 2009; Colaninno & Vourlidas 2009).

(A color version of this figure is available in the online journal.)

in this paper include *SOHO* and *ACE*. They are located at the L1 point, which is along the Sun–Earth line. Using GET_STEREO_LONLAT.pro supplied by the Solar Software, we can get the locations of *STEREO-A* and *STEREO-B* in the heliographic coordinate system. They are S05W21 and S00E20, respectively. The propagation direction of this CME is estimated to be E64 and E51, respectively, by the mass model and forward model of the CME (Thernisien et al. 2009; Colaninno & Vourlidas 2009), as shown in this figure.

At 09:54 UT on 2008 January 2, LASCO/C2 observed an eruption. It is a partial halo CME in LASCO's FOV with a projected angular width of 143° and a linear speed of 676 km s^{-1}. It propagates eastward along a central position angle (CPA) of 85° (relative to the solar north) with a positive acceleration of 22.7 m s^{-2}. For more information about LASCO's observations of this CME, see CDAW Data Center's CME catalog (http://cdaw.gsfc.nasa.gov/CME_list/UNIVERSAL/2008_01/univ2008_01.html). The solar activity level is low in this period, and it is possible to confidently identify the source information and related activities of this event. As reported by the NOAA/Space Weather Prediction Center, there is only one flare on this day, so we assume that it is associated with the CME. This is a long duration C1.2 flare with an X-ray flux enhancement beginning at 06:51 UT, reaching the maximum at 10:00 UT and ending at 11:23 UT. The region slowly decays to a spotless plage on January 5 (see prf1688.pdf in http://www.swpc.noaa.gov/ftpdir/warehouse/2008/2008_WeeklyPDF.tar.gz). The location of AR 10980 on 2008 January 2 was recognized as S07E69 by SolarMonitor, which is hosted at the Solar Physics Group, Trinity College, Dublin and at NASA Goddard Space Flight Center's Solar Data Analysis Center (http://www.solarmonitor.org/region.php?date=20080102region&=10980). There is a global-scale diffuse coronal wave associated with this CME event, which can be readily identified from looking at Extreme Ultraviolet Imaging Telescope (EIT) running difference movies (such as those available at: http://www.ias.u-psud.fr/eit/movies/). This kind of diffuse coronal wave typically maps the footprint of CMEs with large angular widths. Figure 2 gives the extreme ultraviolet (EUV) observations of the Sun from *SOHO*/EIT and *STEREO*/EUVI at the flare maximum time. The different angles between this active region and the various lines of sight make it look different in the observations of these spacecraft. A noticeable fact is that the longitudinal difference between AR 10980 and *STEREO-A* in the heliographic coordinate system is 21° + 69° = 90°, while the latitudinal difference between them is only 7° − 5° = 2°. Therefore, the erupting direction of the CME is likely perpendicular to the Sun–observer line for *STEREO-A*. In other words, the main propagating direction of the CME may be on the POS of *STEREO-A*. The right panel of Figure 2 also supports this conclusion since the source region is located on the east limb.

Figure 3 shows near simultaneous running difference images of the CME as observed by *SOHO*/LASCO and *STEREO*/SECCHI. The coronagraphs onboard these spacecraft have different fields of view (FOVs)—COR1: 1.5–4 Rs; COR2: 2.5–15 Rs; C2: 2–6 Rs; and C3: 3.7–32 Rs. The CME first comes into the FOV of COR1-A, COR1-B, and C2, respectively, at 09:05 UT, 09:15 UT, and 09:54 UT. The CME is mainly propagating 90° east of the observation line of *STEREO-A*. Therefore, it is expected that *STEREO-A* detects the CME a little earlier than *STEREO-B*.

Figure 4 displays a running difference image of the CME from the HI1 instrument onboard *STEREO-A*. HI1 is a heliospheric imager that incorporates sufficient baffling to eliminate enough scattered light so that the passage of CMEs through the heliosphere can be detected. It has a 20° FOV (4°–24° along the Sun–Earth line) and is off-pointed from the Sun center by 14.°0 (Eyles et al. 2009). If the elongation effect is neglected, it can track CMEs from 15 to 90 solar radii approximately. The time cadence of HI1 is 40 minutes. The HI instruments provide

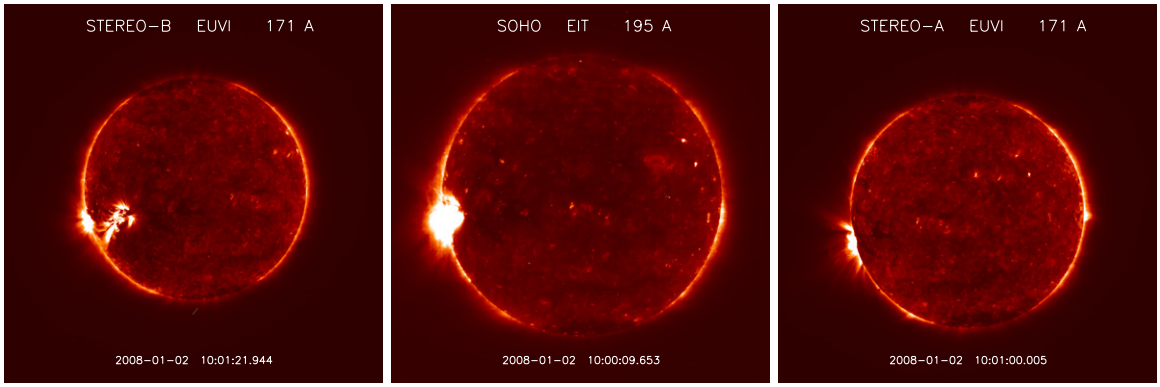

Figure 2. EUV images of the Sun at the flare maximum by *STEREO-B*/EUVI (left), *SOHO*/EIT (middle), and *STEREO-A*/EUVI (right).

(A color version of this figure is available in the online journal.)

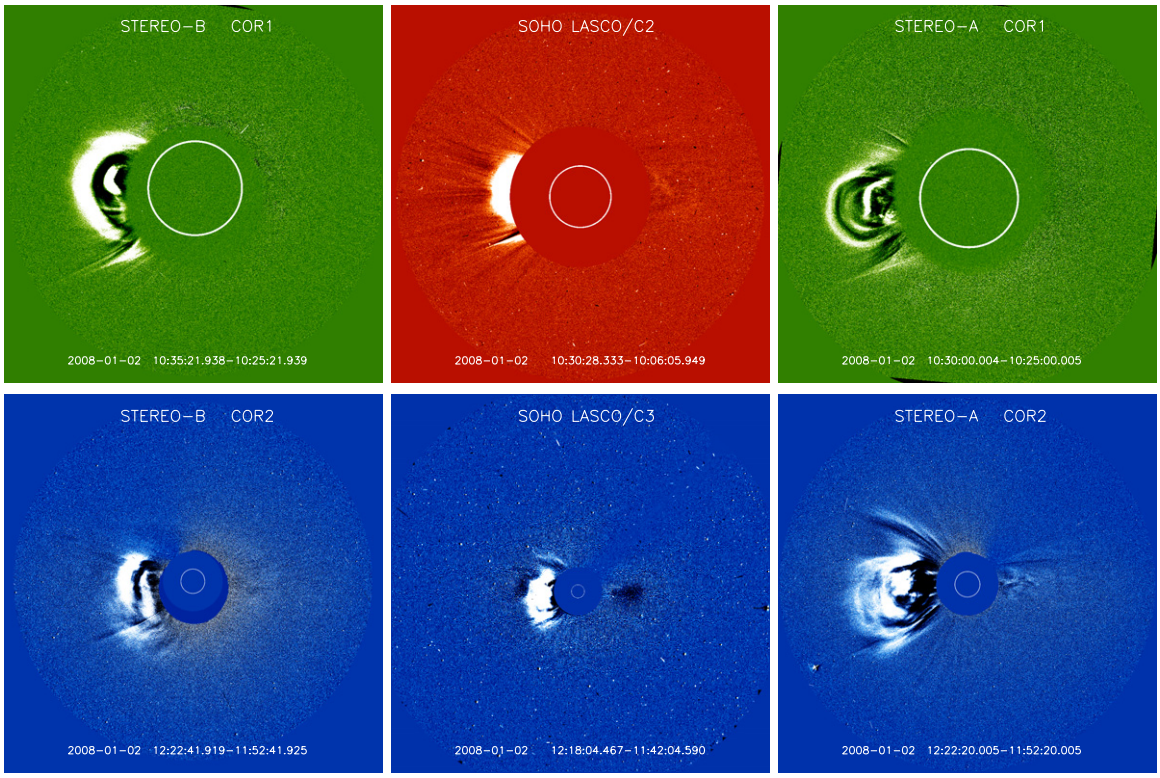

Figure 3. Running-difference images of the 2008 January 2 CME observed by *STEREO*/SECCHI and *SOHO*/LASCO. Top row: images from *STEREO-B*/COR1 (left), LASCO/C2 (middle), and *STEREO-A*/COR1 (right); bottom row: image from *STEREO-B*/COR2 (left), LASCO/C3 (middle), and *STEREO-A*/COR2 (right). The white circle represents the size and location of the solar disk.

(A color version of this figure is available in the online journal.)

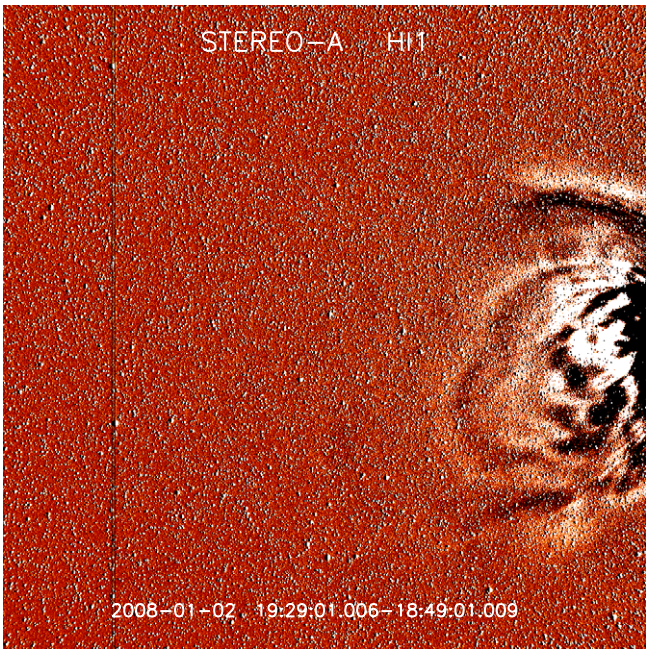

Figure 4. Running-difference image of the 2008 January 2 CME observed by the HI1 instrument onboard *STEREO-A*. The Sun is to the right. The vertical dark lines denote the saturation spikes caused by bright planets and/or stars.

(A color version of this figure is available in the online journal.)

important new opportunities for the observations and studies of CMEs. As for the other camera of the HI instrument, i.e., HI2, we find that the data quality is not good enough for the tracking of this CME, so we do not include the observations of HI2 in this paper.

3. KINEMATIC ANALYSIS

3.1. Tracking the CME

We track the leading edge of the main body of the CME. Here, the "main body" refers to the integrated bright bulk of the CME. From running difference images of all three spacecraft, the leading edge of the main body is chosen and traced manually with a mouse along fixed PAs as the CME propagates outward. Although this tracking can inevitably incorporate judgment uncertainties into the results, it is an effective way in CME tracking at present and is often adopted for studying the kinematics of CMEs (Sheeley et al. 1999; Liu et al. 2009; Temmer et al. 2009). Figure 5 gives an example of tracking the CME leading edge from observations of COR1 on *STEREO-B*. The main body of the CME is clear and looks like a circular arc. The black dots are drawn along the CME front at the fixed PAs between 46° and 132°.

Figure 6 shows the evolution of the leading edge of the CME observed by the four different instruments. The spacecraft located at different vantage points observed different CME shapes. For *STEREO-A* the CME is like a bubble with an angular width of about 50°–70°, while for *STEREO-B* it is not so well-organized or symmetric with an angular width of 80°–90°, wider than that observed by *STEREO-A*. As for LASCO, the CME has an angular width of around 70°–80°, between the angular widths observed by *STEREO-A* and *STEREO-B*. The narrowest width in the *STEREO-A* coronagraphs imply that the propagation direction of the CME is closest to the sky plane of *STEREO-A* among the three spacecraft. This is consistent with the fact that the CME source region is located 90° east of the observation line of *STEREO-A* as discussed in Section 2.

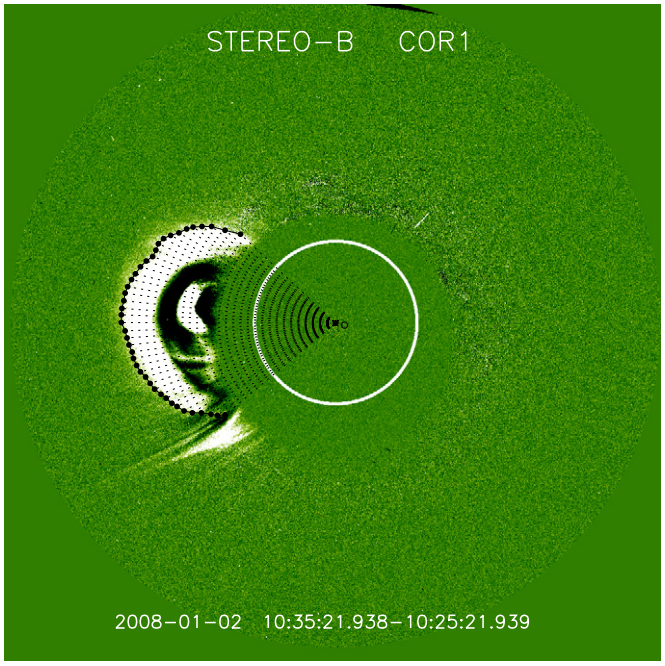

Figure 5. Example of tracking the CME leading edge. The black dots are manually drawn along the CME front at the fixed PAs of 46°, 48°, through 132°. The PA is measured counterclockwise from the solar north. "O" is the center of the Sun, and the white circle represents the solar disk.

(A color version of this figure is available in the online journal.)

Figure 7 displays the elongation–PA plots at different times derived from the observations of these three spacecraft. The elongations at different PAs are not uniform, which indicates that the CME expansion is not spherical when it propagates outward. The PA of the maximum elongation shifts from 90° to 110°, so the CME is deflected southward during its propagation.

Figure 8 shows the variation of the observed angular width of the CME. The maximum projected angular width from *STEREO-B* is the widest (about 90°), the maximum angular width observed by *STEREO-A* is the narrowest (70°), and that observed by *SOHO*/LASCO lies in between (around 80°). The angular width increases rapidly in the observations of COR1 (*STEREO-A&B*) and C2 (*SOHO*). Although it may be partly explained by the occulting of the coronagraphs, this fast increase of the angular width shows a rapid lateral expansion of the CME at the early stage, which is consistent with the finding for the 2007 December 31 CME by Liu et al. (2009) and Dai et al. (2010). These two CMEs have the same source of active region. Also, it is worth noting that this lateral expansion of CMEs has been the focus of some recent studies (Thompson et al. 2000; Attrill et al. 2007, 2009; Veronig et al. 2008; Aschwanden et al. 2009; Cohen et al. 2009; Kienreich et al. 2009). As for the HI1A observations, the angular width of the CME increases slowly and reaches a final width of about 70°.

Figure 9 gives the elongation of the CME front along PA = 100° observed by the three spacecraft. The elongation observed by *STEREO-A* is greater than that from LASCO all the time, while the latter exceeds that measured by *STEREO-B*, which again indicates that the CME is propagating in the POS of *STEREO-A*.

3.2. Correction of Projection Effects

In the projected images, distances from the Sun are measured in terms of the elongation angle ϵ, which is defined as the angle of the observed feature with respect to the Sun–observer line. The conversion from elongation to radial distance is not an easy task in deriving the CME kinematics in three dimensions. In the near Sun region, the "Point-P Method" (abbreviated as PP) supplies a lower-limit estimate of the CME distance (Howard et al. 2006; Kahler & Webb 2007). The primary assumption of this method is that the brightest part of a CME is due to the column density along a Sun-centered spherical front or shell. Point P is the region of the maximum Thomson scattering strength for the observer. This method yields the radial distance R,

$$R = d \sin \epsilon. \quad (1)$$

Here, d is the distance of the observer from the Sun. This model works well especially for very wide CMEs.

The "Fixed-ϕ Method" (abbreviated as Fϕ) is another approach to infer the radial distance of CMEs. It assumes that the CME is a relatively compact structure moving radially away from the Sun at an angle, ϕ, relative to the Sun–observer line (Sheeley et al. 1999; Kahler & Webb 2007). In this case,

$$R = \frac{d \sin \epsilon}{\sin(\epsilon + \phi)}. \quad (2)$$

The parameter ϕ can be determined from the source location of the associated solar flare or by fitting the tracks in time-elongation maps (e.g., Sheeley et al. 1999).

Howard et al. (2007) gave a 3D treatment for the conversion from elongation to radial distances. In their method, the radial distance R of any measured point P can be derived as

$$\frac{d}{R} = \sin \alpha \cot \epsilon + \sin \theta \cos \varphi. \quad (3)$$

Here, θ and φ are the colatitude and longitude of the vector $\boldsymbol{OP}$ (O denotes the Sun center) in the heliocentric Earth-ecliptic coordinate system relative to the Sun–observer line; α is the angle subtended by P at the Sun, i.e., $\angle SOP$ (S stands for spacecraft, i.e., observer). The value of α can be derived in terms of θ and φ, i.e., $\cos \alpha = \sin \theta \cos \varphi$. Details about the derivation of Equation (3) can be found in Howard et al. (2007). The observations of coronagraphs are often expressed in the coordinates of (PA, ϵ). If the CME is located 90° to the Sun–observer line, such as the observations of *STEREO-A* in our case, we have $\varphi = 90°$, $\alpha = 90°$, and $\theta = -$PA. Therefore, Equation (3) is reduced to

$$R = d \tan \epsilon. \quad (4)$$

In order to compare the efficiency of these models, we apply both the PP and Fϕ methods to the observations of COR1 and COR2 of *STEREO* and C2 and C3 of *SOHO*. Due to the limb location of *STEREO-A*, Equation (4) is also applied to the observations of the COR1A and COR2A instruments. We use the location of the associated flare to estimate the propagating direction of this CME (i.e., the angle ϕ in the Fϕ relative to these three spacecraft). It is 49° for *STEREO-B*, 69° for *SOHO*, and 90° for *STEREO-A*. The results are displayed in Figure 10. The two blue curves in this figure are the converted distances from the observations of COR1 and COR2 of *STEREO-B* using the PP and Fϕ, respectively. The red curves represent the distances derived from the observations of LASCO/(C2 and C3) using the PP and Fϕ. For *STEREO-A* $\phi = 90°$, so Equation (2) is the same as Equation (4). The converted distances from COR1A and COR2A data using Equation (4) and the Fϕ are shown by the black solid curve. The results of the PP to COR1A and

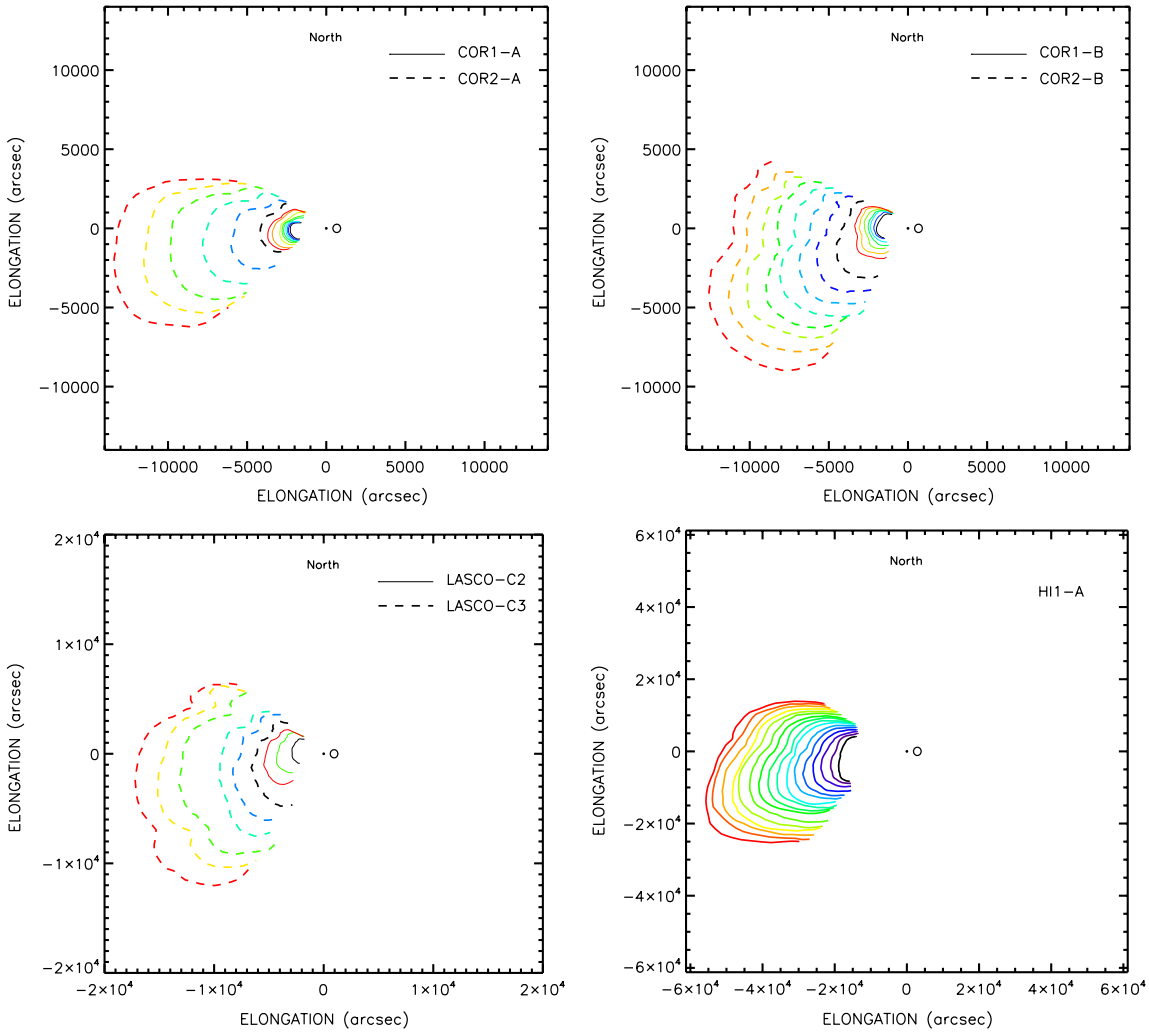

Figure 6. Evolution of the leading edge of the CME observed by COR1 and COR2 of *STEREO-A* (top left), COR1 and COR2 of *STEREO-B* (top right), C2 and C3 of *SOHO* (bottom left), and HI1 of *STEREO-A* (bottom right). The contours denote the CME front at different times.

(A color version of this figure is available in the online journal.)

COR2A are denoted by the scattered asterisks, which are nearly the same as the results of the Fϕ and Equation (4) due to the fact $\sin\epsilon \approx \tan\epsilon$ for small elongation ϵ. For observations from the same instrument, the distance converted from the Fϕ is always larger than that from the PP; for the three spacecraft, the distance observed by *STEREO-A* is the largest, the distance observed by *STEREO-B* is the smallest, and that observed by *SOHO* lies in between. The application of Equation (4) and the Fϕ to *STEREO-A* gives the largest distance, which is taken as the actual distance of the CME front because the projection effect is minimum in this case. The Fϕ works better than the PP for this CME.

Equation (4) or the Fϕ is also applied to the observations of HI1A. The combination of the conversion results from COR1A, COR2A, and HI1A by using Equation (4) (or Fϕ) is shown in the top panel of Figure 11. The solid lines in this panel are the fitting curves to these distances

$$\begin{cases} s = 2.06t^3 - 61.87t^2 + 621.86t - 2084.51, & t \leqslant 10.74\,\mathrm{hr}, \\ s = 4.09t - 39.92, & t > 10.74\,\mathrm{hr}. \end{cases} \quad (5)$$

Here, s is in units of solar radii, t is in units of hours, and the $t = 0$ time is 00:00 UT on 2008 January 2. The derivative of distance s gives the velocity of the CME's leading edge:

$$\begin{cases} v = 1191.2t^2 - 23906.1t + 120139.0, & t \leqslant 10.74\,\mathrm{hr}, \\ v = 789.8, & t > 10.74\,\mathrm{hr}. \end{cases} \quad (6)$$

The velocity is in units of km s^{-1}. The middle panel of Figure 11 shows the velocity of the CME front. The data points represent the velocities that are computed from the adjacent distance measurements using a numerical differentiation with three-point Lagrangian interpolation. This computation method often leads to large variations in the results. The solid curves in the middle panel denote the fitting Equation (6). Although the velocities exhibit some fluctuations, the following trend can be found: the velocity increases rapidly from 200 km s^{-1} at 2.2 Rs (the first tracking point of COR1) to 790 km s^{-1} at about 3.7 Rs; then it remains nearly constant at 790 km s^{-1}. Note that our results about the CME kinematics are only a coarse estimate. As the CME propagates outward, the observed leading edge is not necessarily following the same part of the CME structure, which induces uncertainties in our tracking. The fitting function we adopt may also affect our conclusion about the kinematic expansion of the CME. The acceleration is shown in the lower panel of Figure 11. Similarly, the scattered points denote the accelerations computed from

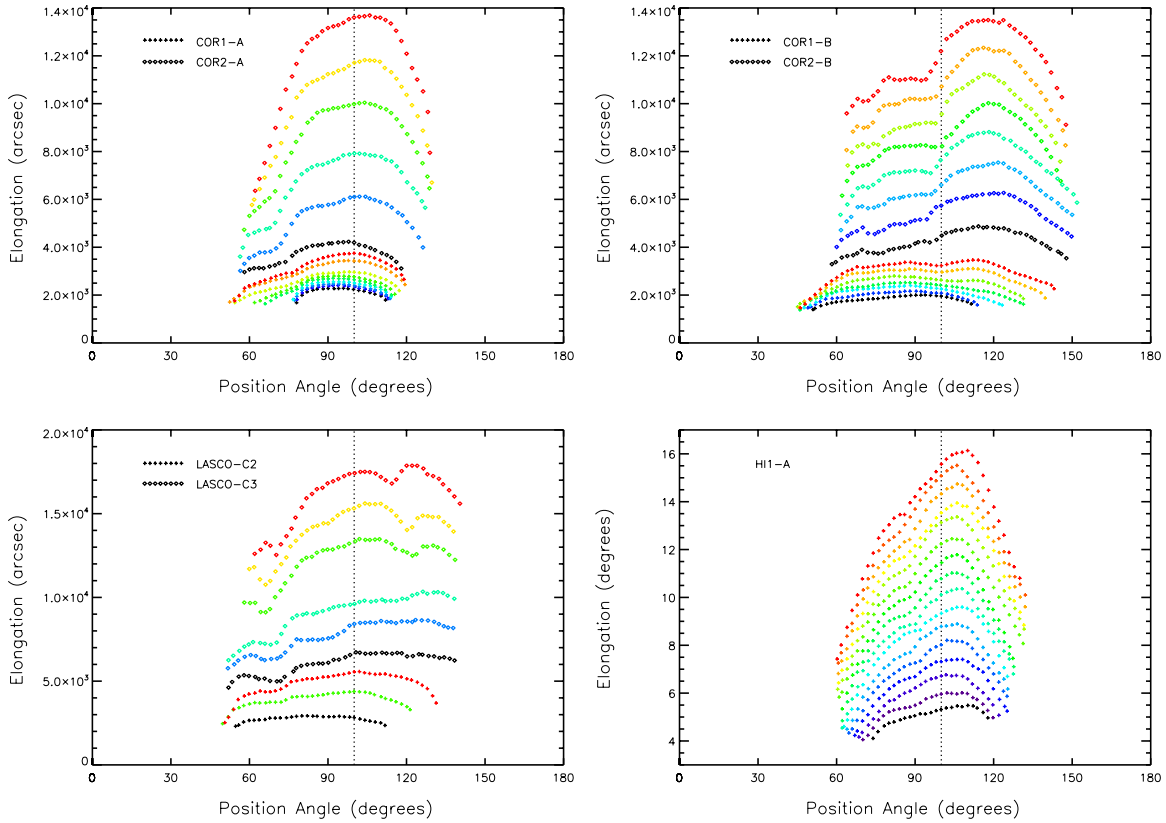

Figure 7. Elongation–PA plots of the CME derived from the observations of COR1 and COR2 of *STEREO-A* (top left), COR1 and COR2 of *STEREO-B* (top right), C2 and C3 of *SOHO* (bottom left), and HI1 of *STEREO-A* (bottom right). The contours from lower to upper denote the CME front at different times. The vertical dotted line stands for the location of PA = 100°.

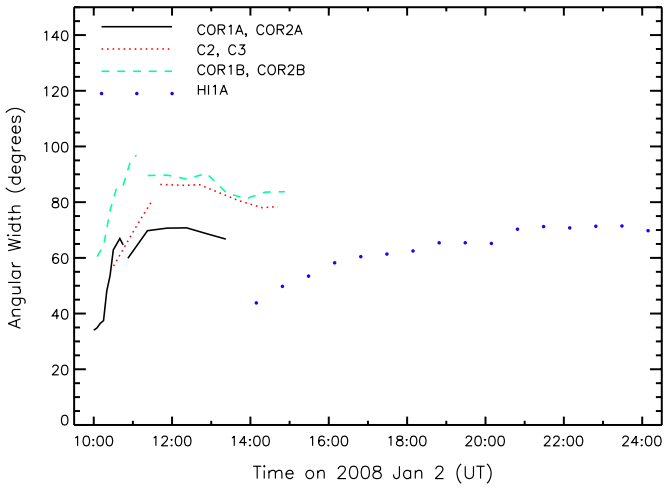

Figure 8. Variation of the projected angular width of the CME observed by the three spacecraft.

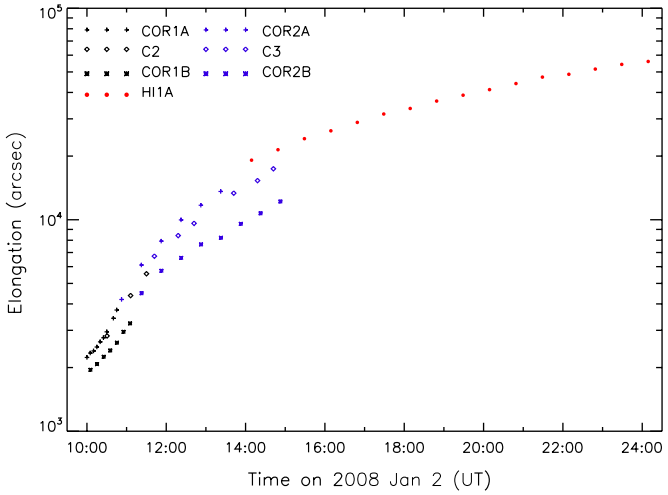

Figure 9. Elongation of the CME front at PA = 100° as a function of time.

adjacent distance measurements (second-order differentiation), and the solid curves denote Equation (7):

$$\begin{cases} a = 661.8t - 6640.6, & t \leqslant 10.74\,\mathrm{hr}, \\ a = 0, & t > 10.74\,\mathrm{hr}. \end{cases} \quad (7)$$

The acceleration is not constant at the early stage but increases significantly. At a height of about 3.7 Rs, the driving force may balance the resistance, so the CME then moves at a constant speed. Similarly, Moore et al. (2007) point out that beyond some height in or below the outer corona the CME plasmoid is in lateral pressure balance with the surrounding magnetic field. The X-ray flux observed by *GOES* 11 for the associated flare is also plotted in the lower panel of Figure 11. An interesting finding is that the acceleration phase of this CME starts near the X-ray flux maximum time (10:00 UT), and stops roughly 45 minutes later (10:45 UT). This means that the acceleration phase of this CME corresponds to the flash phase of the associated flare. It is worthy to note that the acceleration development of this CME and its consistency with the associated flare phase are very similar to the 1998 June 11 CME as studied by Zhang et al. (2001, 2004). These correlations indicate

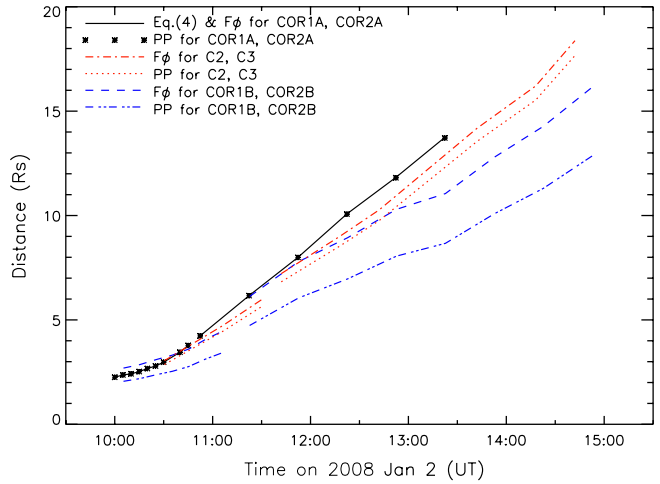

Figure 10. Distance vs. time plots for the leading edge of the CME along PA = 100°, computed using different methods to derive the conversion from measured elongation to real distance from Sun-center. "PP" refers to the "Point-P Method" of Equation (1), and "Fϕ" refers to the "Fixed-ϕ Method" of Equation (2).

(A color version of this figure is available in the online journal.)

that the CME large-scale acceleration and the flare particle acceleration are strongly coupled physical phenomena occurring in the corona (Zhang et al. 2004). The kinematics of this CME are different from those of the 2008 February 4 CME studied by Wood et al. (2009a) and the 2008 May 17 CME by Wood et al. (2009b). In their cases, the CMEs had an initial constant acceleration, then a deceleration, and finally a constant velocity. As there are plenty of works on the CME kinematics, here we just show some cases for the purpose of comparison. Furthermore, different CMEs may undergo different kinematic developments (see also Liu et al. 2008).

4. IN SITU MEASUREMENTS

Figure 12 displays the solar wind magnetic filed and plasma parameters at 1 AU observed by *ACE* and *STEREO*. The vertical dashed line in the three panels indicates our estimated arrival time of the CME at 1 AU; the estimate is based on the propagation speed of 790 km s^{-1} and the assumption of no evident deceleration beyond our tracking range. The time interval of the figure starts from January 2 and ends at January 8, a long period covering the CME's beginning and potential arrival time at 1 AU. No obvious ICME signatures are observed during this time interval, such as enhanced helium abundance, depressed proton temperature, and smooth strong magnetic fields compared with the ambient solar wind. It is likely that the CME misses all of these spacecraft at 1 AU. The longitudinal separation between the CME source and *STEREO-A*, *ACE*, and *STEREO-B* is 90°, 69°, and 49°, respectively. The longitudinal extent of the CME may not be large enough to reach the spacecraft. Also, the CME may be deflected eastward by the Parker spiral magnetic field during its propagation in the heliosphere, which will make it even further from these spacecraft. An interesting feature in this figure is a Corotating Interaction Region (CIR) structure observed by all the spacecraft: the proton density, temperature, and magnetic field strength are enhanced when a fast stream overtakes a slower one. The CIR was first observed by *STEREO-B*, then more than one day later by *ACE*, and finally three days later by *STEREO-A*.

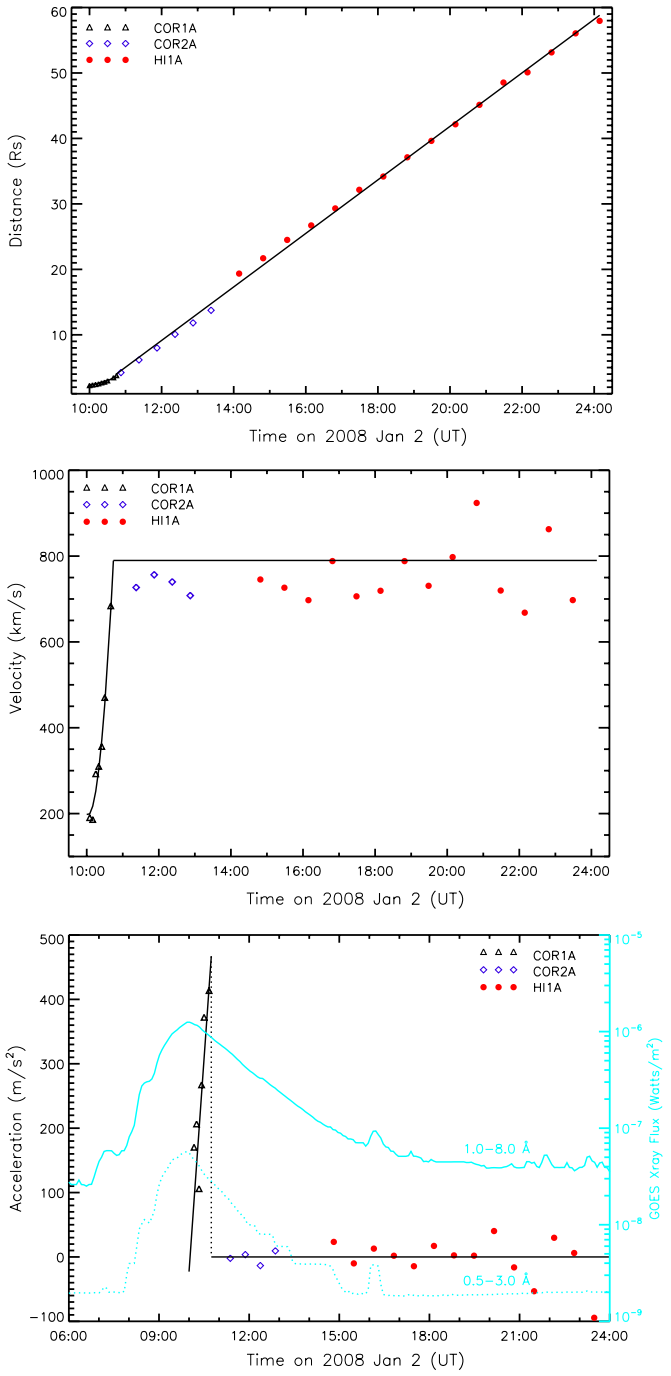

Figure 11. Distance of the leading edge of the CME along PA = 100° as a function of time (using Equation (4) or Fϕ, top panel). The solid curves represent the fitting Equation (5) to the distance measurements. The velocity and acceleration profiles are shown in the middle and bottom panel, where the solid curves represent their fitting equations of (6) and (7). The green curves in the bottom panel denote the *GOES*11 X-ray flux of 1.0–8.0 Å (solid) and 0.5–3.0 Å (dotted), respectively.

(A color version of this figure is available in the online journal.)

5. CONCLUSIONS

Based on the observations of *STEREO* and *SOHO*, we study the morphology and kinematics of the 2008 January 2 CME that occurred during a quiet time of solar activity. Our study demonstrates that the appearance of a CME can be rather different in the observations of the spacecraft located at different points. For *STEREO-A*, the main body of this CME is like a

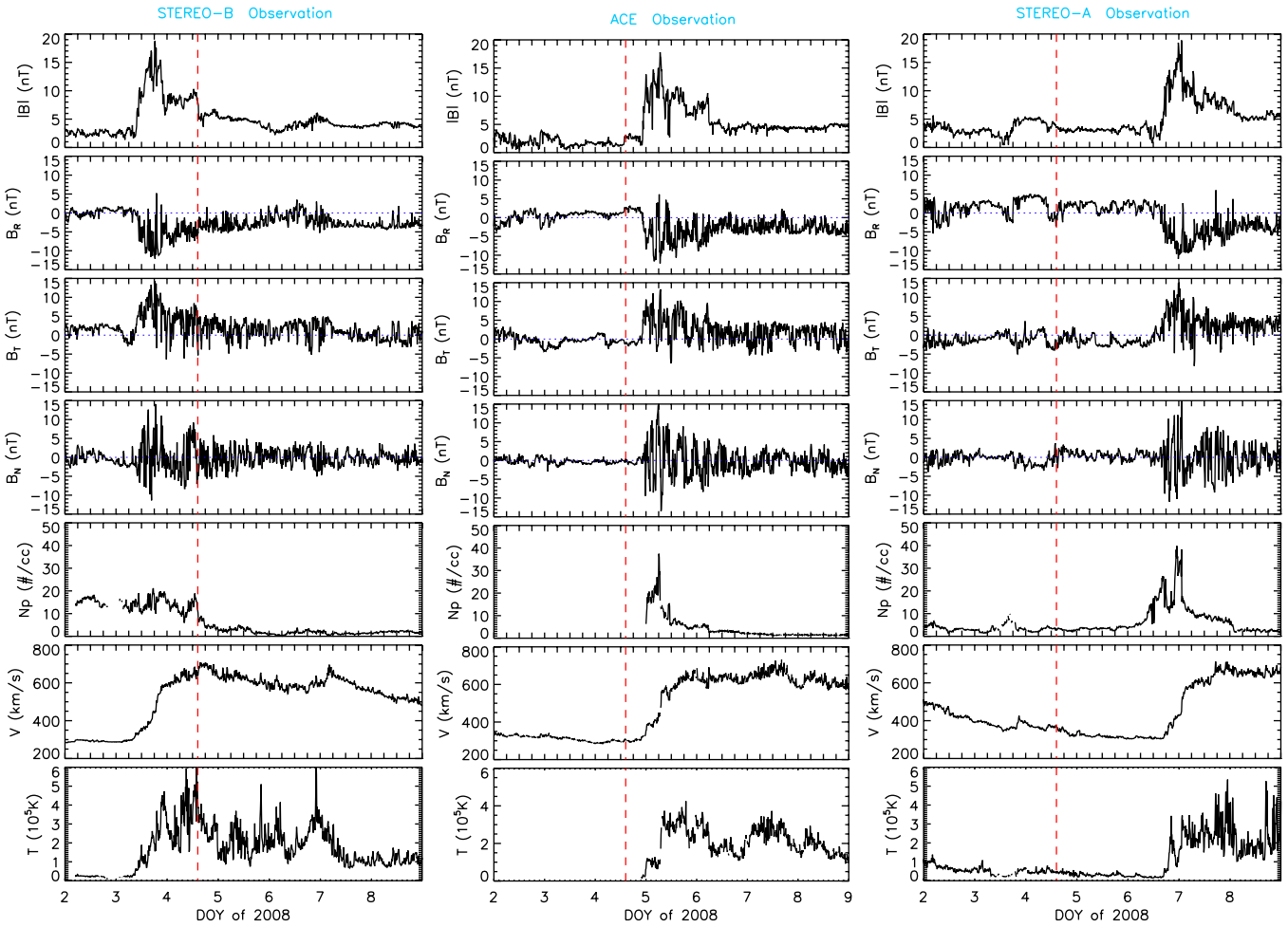

Figure 12. Interplanetary magnetic field (from top to bottom: |B|, B_R, B_T, B_N), proton density, speed, and temperature in the RTN coordinate system from the instruments on *STEREO-B* (left), *ACE* (middle), and *STEREO-A* (right). No ICME signatures are observed during this time interval. A CIR is observed in this period first by *STEREO-B*, then by *ACE*, and last by *STEREO-A*. The vertical-dashed line denotes the predicted arrival time of the CME at 1 AU (i.e., 14:24 UT on January 4). (A color version of this figure is available in the online journal.)

bubble with the angular width of around 50°–70°. It propagates eastward perpendicular to the observation line of *STEREO-A* with somewhat of an expansion, and is deflected a little toward the south hemisphere in its journey. For *STEREO-B* and *SOHO*, the CME looks relatively faint with a dim front edge and wider angular width. These are due to the projection effects. Several methods are used to compute the radial distances of the CME leading edge, including the PP, Fϕ, and a 3D method. The CME was propagating 90° east to the observing line of *STEREO-A*, so the observations of *STEREO-A* provide the best estimate of the true CME kinematics. Our analysis demonstrates that the CME first experiences a rapid acceleration below 3.7 Rs, which corresponds to the flash phase of the associated flare. Then, it moves at a constant speed of 790 km s^{-1} in the inner heliosphere to at least 60 Rs. Because the CME's propagation direction is far away from the spacecraft and exceeding the half angular width of the CME, it does not pass either of the *STEREO* spacecraft or *ACE*.

This CME has also been studied by others. de Koning et al. (2009) applied a geometric localization technique to *STEREO*/COR2 images to derive the 3D characteristics of this CME. They found that the calculated speed of the CME was 640 ± 64 km s^{-1} and the propagating direction was $4° \pm 1°$S and $64° \pm 11°$E. Colaninno & Vourlidas (2009) used a mass method to infer the longitudinal direction of this CME to be $-64°$ with respect to the Sun–Earth line. Our interpretation about the propagating direction of the CME based on the source location of S07E69 is consistent with these results. Our calculated CME speed of 790 km s^{-1} is larger than theirs. In addition, the linear speed of this CME is 676 km s^{-1} as listed in the LASCO catalog in FOVs of C2 and C3; CACTus (the Computer Aided Cme Tracking software) identified this CME in COR2A with a median speed of 510 km s^{-1} and in COR2B with a median speed of 416 km s^{-1}, while the median speed in our tracking results in COR2A is 740 km s^{-1}; SEEDS (Solar Eruptive Event Detection System) gives a linear-fit speed of 350 km s^{-1} from LASCO. All of these are lower than our estimate, presumably because they did not remove the projection effects.

Our work shows a good example of the kinematic tracking and analysis of a CME using multi-spacecraft data including both remote-sensing and in situ observations. This proves to be more comprehensive than previous single spacecraft observations. The results are helpful for understanding the propagation and evolution of CMEs in interplanetary space.

The work is jointly supported by the National Natural Science Foundation of China (40921063, 40704030, 40890162, 40874091, and 40974107), the 973 project under grant 2006CB806304, the Specialized Research Fund for State Key Laboratories, and the Knowledge Innovation Program of the

Chinese Academy of Sciences. S.T.W. is supported by AFOSR (grant FA9550-07-1-0468), AURA Sub-Award C10569A of NSO's Cooperative Agreement AST 0132798, and NSF (grant ATM-0754378). We are very grateful to the anonymous referee for the constructive and helpful comments. We acknowledge the use of data from *SOHO*, *STEREO*, and *ACE* and the data from the "LASCO CME catalog." The *STEREO*/SECCHI data are produced by a consortium of NRL (US), LMSAL (US), NASA/GSFC (US), RAL (UK), UBHAM (UK), MPS (Germany), CSL (Belgium), IOTA (France), and IAS (France). In addition to SECCHI, this work has also made use of data provided by the *STEREO*/IMPACT and PLASTIC teams. We thank the *SOHO*/LASCO team for letting us use their data. *SOHO* is a mission of international collaboration between ESA and NASA. We thank the *ACE*/SWEPAM and MAG instrument teams for providing their data. We thank Dr. Tim Howard and Dr. Hongqiang Song for beneficial discussions.

REFERENCES

Aschwanden, M. J., et al. 2009, ApJ, 706, 376
Attrill, G. D. R., et al. 2007, Astron. Nachr., 328(8), 760
Attrill, G. D. R., et al. 2009, ApJ, 704, 1296
Cohen, O., et al. 2009, ApJ, 705, 587
Colaninno, R. C., & Vourlidas, A. 2009, ApJ, 698, 852
Dai, Y., et al. 2010, ApJ, 708, 913
de Koning, C. A., Pizzo, V. J., & Biesecker, D. A. 2009, Sol. Phys., 256, 167
Eyles, C. J., et al. 2009, Sol. Phys., 254, 387
Frazin, R. A., Jacob, M., Manchester, W. B., IV, Morgan, H., & Wakin, M. B. 2009, ApJ, 695, 636
Harrison, R. A., et al. 2008, Sol. Phys., 247, 171
Howard, R. A., et al. 1985, J. Geophys. Res., 90, 8173
Howard, R. A., et al. 2008, Space Sci. Rev., 136, 67
Howard, T. A., Nandy, D., & Koepke, A. C. 2008, J. Geophys. Res. (Space Phys.), 113, A01104
Howard, T. A., & Tappin, S. J. 2008, Sol. Phys., 252, 373
Howard, T. A., et al. 2006, J. Geophys. Res., 111, A04105
Howard, T. A., et al. 2007, ApJ, 667, 610
Hundhausen, A. J. 1993, J. Geophys. Res., 98, 13177
Kahler, S. W., & Webb, D. F. 2007, J. Geophys. Res., 112, A09103
Kienreich, I. W., Temmer, M., & Veronig, A. M. 2009, ApJ, 703, L118
Liu, Y., Davies, J. A., Luhmann, J. G., Vourlidas, A., Bale, S. D., & Lin, R. P. 2010, ApJ, 710, L82
Liu, Y., Luhmann, J. G., Bale, S. D., & Lin, R. P. 2009, ApJ, 691, L151
Liu, Y., et al. 2008, ApJ, 689, 563
Maloney, S. A., Gallagher, P. T., & James McAteer, R. T. 2009, Sol. Phys., 256, 149
Michalek, G. 2006, Sol. Phys., 237, 101
Michalek, G., Gopalswamy, N., & Yashiro, S. 2003, ApJ, 584, 472
Mierla, M., et al. 2008, Sol. Phys., 252, 385
Moore, R. L., Sterling, A. C., & Suess, S. T. 2007, ApJ, 668, 1221
Sheeley, N. R., Jr., Walters, J. H., Wang, Y. M., & Howard, R. A. 1999, J. Geophys. Res., 104, 24739
St. Cyr, O. C., et al. 2000, J. Geophys. Res., 105, 18169
Temmer, M., Preiss, S., & Veronig, A. M. 2009, Sol. Phys., 256, 183
Thernisien, A., Vourlidas, A., & Howard, R. A. 2009, Sol. Phys., 256, 111
Thompson, B. J., et al. 2000, Geophys. Res. Lett., 27, 1431
Veronig, A. M., Temmer, M., & Vrnak, B. 2008, ApJ, 681, L113
Webb, D. F., et al. 2009, Sol. Phys., 256, 239
Wood, B. E., et al. 2009a, ApJ, 694, 707
Wood, B. E., et al. 2009b, Sol. Phys., 259, 163
Xie, H., Ofman, L., & Lawrence, G. 2004, J. Geophys. Res., 109, A03109
Zhang, J., et al. 2001, ApJ, 559, 452
Zhang, J., et al. 2004, ApJ, 604, 420
Zhao, X. P., Plunkett, S. P., & Liu, W. 2002, J. Geophys. Res., 107, 1223